JACS JOURNAL OF THE AMERICAN CHEMICAL SOCIETY

Article

Cite This: J. Am. Chem. Soc. 2018, 140, 12989−12995

pubs.acs.org/JACS

Colloidal Synthesis of Double Perovskite $Cs_2AgInCl_6$ and Mn-Doped $Cs_2AgInCl_6$ Nanocrystals

Federico Locardi,[†,‡] Matilde Cirignano,[‡] Dmitry Baranov,[‡] Zhiya Dang,[‡] Mirko Prato,[§] Filippo Drago,[‡] Maurizio Ferretti,[†] Valerio Pinchetti,[∥] Marco Fanciulli,[∥] Sergio Brovelli,[∥] Luca De Trizio,*[,‡] and Liberato Manna*[,‡]

[†]Dipartimento di Chimica e Chimica Industriale, Università degli Studi di Genova, Via Dodecaneso 31, 16146 Genova, Italy

[‡]Nanochemistry Department and [§]Materials Characterization Facility, Istituto Italiano di Tecnologia, Via Morego 30, 16163 Genova, Italy

[∥]Dipartimento di Scienza dei Materiali, Università degli Studi di Milano-Bicocca, via R. Cozzi 55, 20125 Milano, Italy

Supporting Information

ABSTRACT: We show here the first colloidal synthesis of double perovskite $Cs_2AgInCl_6$ nanocrystals (NCs) with a control over their size distribution. In our approach, metal carboxylate precursors and ligands (oleylamine and oleic acid) are dissolved in diphenyl ether and reacted at 105 °C with benzoyl chloride. The resulting $Cs_2AgInCl_6$ NCs exhibit the expected double perovskite crystal structure, are stable under air, and show a broad spectrum white photoluminescence (PL) with quantum yield of ∼1.6 ± 1%. The optical properties of these NCs were improved by synthesizing Mn-doped $Cs_2AgInCl_6$ NCs through the simple addition of Mn-acetate to the reaction mixture. The NC products were characterized by the same double perovskite crystal structure, and Mn doping levels up to 1.5%, as confirmed by elemental analyses. The effective incorporation of Mn ions inside $Cs_2AgInCl_6$ NCs was also proved by means of electron spin resonance spectroscopy. A bright orange emission characterized our Mn-doped $Cs_2AgInCl_6$ NCs with a PL quantum yield as high as ∼16 ± 4%.

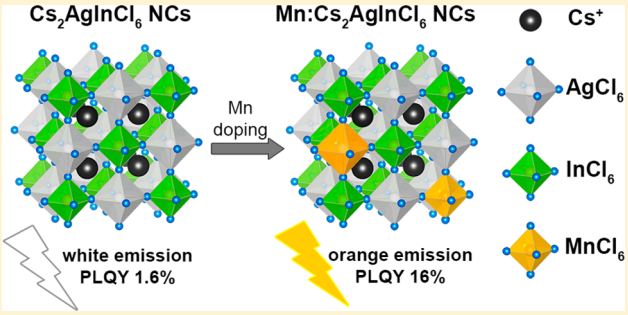

INTRODUCTION

In the past decade, research on $APbX_3$ (where A = $CH(NH_2)_2^+$, $CH_3NH_3^+$, Cs^+; X = Cl^-, Br^-, I^-) perovskite nanocrystals (NCs) has experienced a steep growth. These materials, on the basis of their attractive optoelectronic properties, have been widely employed in various devices, such as solar cells, light emitting diodes, and photodetectors.[1,2] Despite their attractiveness, lead halide perovskites have to face important challenges such as the lack of stability upon prolonged exposure to light, humidity, or high temperature, and, of particular importance, the intrinsic toxicity (and its bioaccumulation in the ecosystem) of lead.[3−9] Such issues are nowadays motivating the materials science community to find alternative stable and environmentally sustainable metal halide perovskite NC systems with comparable optoelectronic properties.[9−14]

To obtain lead-free metal halide compounds one strategy consists in the "simple" substitution of Pb^{2+} cations with other less toxic divalent metal ions of the same group IV, such as Sn^{2+} or Ge^{2+}.[15] Unfortunately, the corresponding materials have been shown to suffer from the oxidation of both Sn^{2+} and Ge^{2+} to their respective 4+ states, resulting in a poor stability.[4] One of the most promising strategies that is currently pursued is based on the replacement of two divalent Pb^{2+} ions with one monovalent M^+ and one trivalent M^{3+} cation, i.e., $2Pb^{2+} \rightarrow M^+ + M^{3+}$, generating quaternary $A_2M^+M^{3+}X_6$ compounds, also called double perovskites (DPs), which maintain both the 3D perovskite crystal structure and the charge neutrality.[16] The emergence of such materials, historically known as elpasolites, dates back to the end of the 1960s, when a large number of $A_2M^+M^{3+}X_6$ compounds (where A and M^+ = Li^+, Na^+, K^+, Rb^+, Cs^+, Ag^+, Tl^+, etc.; M^{3+}= Bi^{3+}, Al^{3+}, Ln^{3+}, Ga^{3+}, Fe^{3+}, etc.; X = F^-, Cl^-, Br^-, I^-) have been reported as ferroelectric materials.[17−19]

Among the possible DP materials, $Cs_2AgBiBr_6$ and $Cs_2AgBiCl_6$ have been recently proposed as candidates for photovoltaic applications,[3,8,20−27] also because they exhibit good stability in air. On the other hand, it emerged that such systems are characterized by a very low photoluminescence (PL) emission and low power conversion efficiency (2.2%) in PV devices,[28] most likely as a consequence of their indirect bandgap.[3,6,8,20−27,29−33] New alternative direct-bandgap DP systems are, thus, currently under the spotlight.[23] Several computational studies, aimed at screening different $A-M^+-M^{3+}-X$ combinations, predicted that numerous stable DP

Received: July 27, 2018
Published: September 10, 2018

DOI: 10.1021/jacs.8b07983
J. Am. Chem. Soc. 2018, 140, 12989−12995

compounds should exhibit a direct bandgap spanning the spectral range relevant for solar energy conversion (1.5−2.5 eV), including Cs_2AgInX_6, Rb_2AgInX_6, and Rb_2CuInX_6 (X = Cl, Br).[34,35]

After the pioneering work of Volonakis et al. in 2016,[8] different groups reported the synthesis of bulk $Cs_2AgInCl_6$, which is characterized by a DP structure (with space group $Fm\bar{3}m$) at room temperature, a fundamental direct band gap of ∼2 eV (reported values range from 2.1 to 2.6 eV), long carrier lifetimes (6 μs), and excellent moisture, light, and heat stability, which make it a promising alternative to Pb-based halide perovskites.[7,23,30,34,36−39] DFT calculations have revealed that this material is characterized by a flat valence band maximum (VBM), originating from Ag 4d and Cl 3p orbitals, and a dispersive conduction band minimum (CBM), deriving from delocalized In 5s states.[23,30,36] Bulk $Cs_2AgInCl_6$ crystals (single crystals or powder) are white in color, with an optical band gap (Eg_{OPT}) of ∼3.3 eV, and they are characterized by a weak PL emission at around 608 nm.[7,30,36−38] To explain such optical properties, Meng et al. and Zhuo et al., in parallel, calculated that direct VBM to CBM transitions at the Γ point are parity-forbidden.[7,30] This results in optical absorption coefficients that are low at energies close to the fundamental band gap, and the absorption onset falls at energies as high as 3.45 eV, in agreement with the experimental values. Also, because parity-forbidden transitions do not affect the relaxation of the photoexcited carriers, they can relax to the CBM and the VBM, recombining at energies close to that of the fundamental bandgap (2 eV) and leading to a weak PL emission.[37]

In the past year, the high stability and the relatively large Eg_{OPT} of such material motivated Nandha et al. to dope $Cs_2AgInCl_6$ powders with Mn^{2+} ions, to improve the optical properties of the resulting compound.[38] Among different doping approaches to both II−VI semiconductors and halide perovskite NCs,[40−44] the most studied has been, indeed, the Mn doping of wide band gap semiconductor hosts.[45] In such systems, the photoexcited host transfers its energy to Mn ions promoting electronic transitions between atomic d-orbitals, resulting in yellow-orange d−d emission.[40,42,43,45] The PL from such color-centered impurities (i.e., Mn^{2+} ions) is characterized by long lifetimes, high PL quantum yield (QY), and a large Stokes shift, which minimizes the self-absorption of the system.[45−49] In fact, in Mn-doped $Cs_2AgInCl_6$ powders (having 0.9% of Mn^{2+} ions) orange emission was observed at ∼630 nm, with a PLQY around 3−5%, making this material an interesting Pb-free DP.[38]

Unfortunately, as underlined by Jodlowski et al.,[5] the main problem of current DP synthetic approaches relies on the difficulty of fabricating crystalline thin films using solution processing methods, limiting the implementation of such materials in devices, for example solar cells.[27] This was ascribed to the poor solubility of precursors used for the synthesis of DP materials (i.e., metal halide salts), which makes it difficult to prepare high-quality films. In this regard, the use of a colloidal approach to fabricate DP NC samples, which can be subsequently deposited as a thin film, appears as an interesting alternative.[50−53]

Here we report a colloidal synthesis of $Cs_2AgInCl_6$ NCs with good control over the size distribution of the final product. This was achieved by employing a new colloidal route that we recently proposed for the synthesis of both all-inorganic and hybrid organic−inorganic $APbX_3$ NC systems.[54] In this approach, metal carboxylate precursors (Cs-oleate, Ag- and In-acetates) are mixed together with ligands (oleic acid and oleylamine), and a solvent (diphenyl ether) and heated to the desired temperature; the nucleation and growth of NCs is then triggered by the swift injection of benzoyl chloride (see Scheme 1). By tuning the Cs/Ag/In/Cl precursor ratio, we could regulate the reactivity of the different cations toward Cl anions, so that phase-pure DP $Cs_2AgInCl_6$ NCs could be synthesized. The NCs exhibited good stability up to 500 °C and under air, and white PL emission, with poor PLQY (1.6%). To improve the optical properties of such NCs, we prepared Mn-doped $Cs_2AgInCl_6$ NC samples, by simply adding Mn-acetate to the initial reaction mixture. The synthesized NCs retained the DP crystal structure of parental $Cs_2AgInCl_6$ ones, and they exhibited a bright orange PL emission having a QY as high as ∼16%.

Scheme 1. Colloidal Synthesis of Double Perovskite $Cs_2AgInCl_6$ and Mn-Doped $Cs_2AgInCl_6$ Nanocrystals

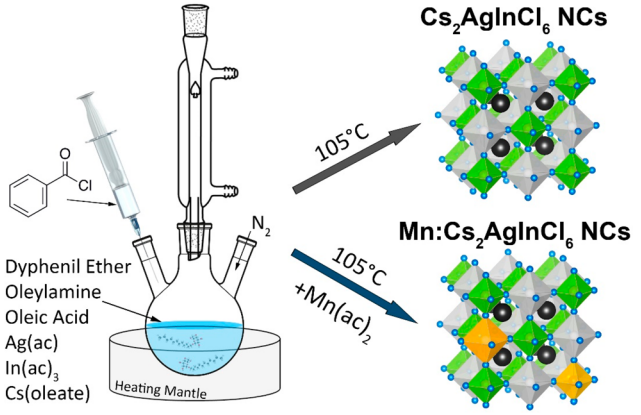

EXPERIMENTAL SECTION

Chemicals. Silver acetate (Ag(ac) 99.99%), indium(III) acetate ($In(ac)_3$ 99.99%), manganese acetate ($Mn(ac)_2$, 99.99%), cesium carbonate (Cs_2CO_3, reagent plus 99%), oleic acid (OAc, 90%), oleylamine (Olam, 70%), benzoyl chloride (Bz-Cl, 98%), and diphenyl ether (DPE, 99.5%) were purchased from Sigma-Aldrich. All chemicals were used without any further purification.

Preparation of Cesium Oleate. The reaction was performed in a three-neck flask under inert atmosphere. A 0.5 M Cs-oleate solution was prepared by mixing cesium carbonate (1630 mg) with OAc (20 mL). The mixture was first degassed under vacuum at 100 °C for 30 min and subsequently heated to 150 °C under N_2 flux for 3 h, until the solution became clear. The resulting product was cooled to room temperature and stored in a vial under air.

Synthesis of Undoped and Mn-Doped $Cs_2AgInCl_6$ NCs. In a typical synthesis, Ag(ac) (0.24 mmol), $In(ac)_3$ (0.25 mmol), 0.5 mL of Olam, 1 mL of the Cs-oleate solution, and 4 mL of DPE were loaded in a three-neck flask and dried under vacuum for 30 min at 40 °C. Subsequently, the system was flushed under N_2, the temperature was increased to 105 °C (at 10 °C/min), and, at that temperature, 200 μL of Bz-Cl (1.72 mmol), mixed with 0.5 mL of degassed DPE, was swiftly injected into the flask. The reaction was quenched after 5 s by cooling with an ice−water bath. The product solution was centrifuged at 4500 rpm for 10 min, the supernatant was discarded, and precipitated NCs were redispersed in 3 mL of hexane. Mn-doped $Cs_2AgInCl_6$ samples were prepared using the same protocol, but employing a slightly lower amount of Ag(ac) (0.22 mmol) and adding a desired amount of $Mn(ac)_2$ to the starting reaction mixture. Three different Mn-doped samples were prepared by using Mn/In precursor ratio of 0.1, 0.2, and 0.3.

DOI: 10.1021/jacs.8b07983
J. Am. Chem. Soc. 2018, 140, 12989−12995

Inductively Coupled Plasma (ICP-OES) Elemental Analysis. ICP elemental analysis was carried out via inductively coupled plasma optical emission spectroscopy (ICP-OES) with an iCAP 6300 DUO ICP-OES spectrometer (ThermoScientific). All chemical analyses performed by ICP-OES were affected by a systematic error of about 5%. The samples were dissolved in nitric acid (HNO_3 68% (v/v)) and heated to 180 °C for 45 min in a microwave reactor (CEM MARS5). After this step, Cs^+, Mn^{2+}, and In^{3+} ions were dissolved in the acid solution, while AgCl precipitated, due to its very low solubility. The AgCl white solid was thus separated from the acid solution via centrifugation. The supernatant was diluted using Milli-Q water and analyzed, without any further operations, to determine the concentration of Mn^{2+} and In^{3+} ions. It is worth noting here that no traces of Ag^+ ions were detected in this solution. The AgCl precipitate, on the other hand, was reacted with ammonia (0.5 mL of NH_3 solution in water) to form water-soluble complexes,[55] which were diluted with Milli-Q water and analyzed.

UV−vis Absorption, PL and PL Quantum Yield (QY) Measurements. The UV−visible absorption spectra were recorded using a Varian Cary 300 UV−vis absorption spectrophotometer. The PL and PL excitation (PLE) spectra of Mn-doped samples were measured on a Varian Cary Eclipse spectrophotometer. The PL and PLE spectra of undoped $Cs_2AgInCl_6$ NCs were recorded with a FLS920 Edinburgh Instruments spectrofluorimeter in a 90° geometry. The samples were excited with 300 nm output of the continuous xenon lamp (Xe900). The excitation slit width was set at 5 nm, the detection slit width was set at 1.75 nm, and the spectra were recorded with 2 nm steps. The PL spectra were collected over a 400−850 nm spectral range; a "330 nm" long pass filter with a flat transmission of ∼90−91% in that spectral range was placed between the sample and detector to remove the second harmonic of the excitation light. Samples were prepared by diluting NC dispersions in 3 mL of hexane in quartz cuvettes with a path length of 1 cm. The PLQYs were measured using a FLS920 Edinburgh Instruments spectrofluorimeter equipped with an integrating sphere. The samples were excited at 300 nm using the output of the continuous Xe lamp. Complete details of PLQY measurements are described in Supporting Information (SI).

Time-Resolved PL Experiments. Spectroscopic studies were carried out on hexane solutions of NCs. For transient PL measurement, the Mn-doped NCs were excited using a frequency tripled pulsed Nd:YAG laser at 3.49 eV with a 100 Hz repetition rate (pulse duration, 5 ns), and the emitted light was collected with a photon counting unit (resolution better than the pulse duration).

Transmission Electron Microscopy (TEM) Characterization. Bright field TEM (BF-TEM) imaging was performed on a JEOL JEM-1011 microscope equipped with a thermionic gun operating at 100 kV accelerating voltage. For these analyses, the samples were prepared by dropping dilute suspensions of NCs onto carbon-coated 200 mesh copper grids. High-resolution TEM (HRTEM) imaging, high-angle annular dark field (HAADF)-scanning TEM (STEM) imaging, and energy-dispersive X-ray spectroscopy (EDS) analyses for the undoped sample and the doped sample obtained with a Mn/In precursor ratio of 0.2 were carried out on a JEOL JEM-2200FS microscope equipped with a Schottky emitter working at an accelerating voltage of 200 kV, a CEOS spherical aberration corrector for the objective lens, and a Bruker Quantax 400 system with a 60 mm^2 XFlash 5060 silicon drift detector (SDD). For doped samples obtained using a Mn/In precursor ratio of 0.1 and 0.3, annular dark field (ADF)-STEM imaging and EDS spectra were acquired by a JEOL JEM-1400 plus TEM operating at an acceleration voltage of 120 kV, equipped with a SDD which collects X-rays from samples at an unprecedented large solid angle of up to 0.98 steradians from a detection area of 100 mm^2. For these latter analyses, the NC suspensions were drop-cast onto ultrathin carbon/holey carbon-coated gold grids. The EDS spectra were quantified using the Cliff-Lorimer method for Cs Lα, Ag Lα, In Lα, Cl Kα, and Mn Kα peaks, and the reported STEM-EDS maps were obtained by integrating the intensities over the same peaks.

X-ray Diffraction (XRD) Characterization. The XRD analysis was performed on a PANanalytical Empyrean X-ray diffractometer, equipped with a 1.8 kW CuK_α ceramic X-ray tube and a PIXcel^{3D} 2 × 2 area detector, operating at 45 kV and 40 mA. Specimens for the XRD measurements were prepared by dropping a concentrated NC solution onto a silicon zero-diffraction single crystal substrate. The diffraction patterns were collected under ambient conditions using a parallel beam geometry and the symmetric reflection mode. XRD data analysis was elaborated using the HighScore 4.1 software from PANalytical.

Electron Spin Resonance (ESR) Spectroscopy. The ESR spectra were recorded with a Varian E15 spectrometer and a Bruker super high Q cavity operated at X-band, ∼9.3−9.5 GHz, in the absorption mode. The static magnetic field was modulated at 100 kHz. The microwave frequency ν_0 and the magnetic field $\mathbf{B}_0$ were monitored continuously with an electronic counter and a Hall probe. 1,3-bis phenylene-2-phenyl allyl was used as reference to determine the *g*-factors.

Differential Thermal Analysis/Thermogravimetric and Evolved Gas Analysis (DTA/TG EGA) Characterization. A 200 μL aliquot of each NC sample was put into an alumina crucible and dried at atmospheric pressure and then under vacuum for 5 min. The DTA/TG characterization (LabsysEvo 1600, Setaram) was performed from 35 °C to 1000 °C, heating at 10 °C/min in He (20 mL/min). At every minute the autoinjector, set at 280 °C (Automation), collects for 10 s, in a loop of 1 mL, the evolved gases from the output of DTA/TG. The so-collected molecules are injected into the GC (TraceGC Ultra, Thermo Fisher Scientific) equipped with column Mega-5 (5% phenyl−95% methyl polysiloxane; length 30 m; internal diameter: 0.25 mm; film thickness: 0.25 μm). The oven and the inlet temperatures were set at 200 °C and 280 °C, respectively, and the He carrier gas flux was set at 1.2 mL/min with a split ratio of 1:10 and split flow of 12 mL/min. The GC was coupled to a MS-quadrupole (DSQ I, Thermo Fisher Scientific, operating in the EI mode at 70 eV, ion source at 250 °C, transfer line at 280 °C) that scanned in the 33−200 m/z range.

X-ray Photoelectron Spectroscopy (XPS) Characterization. XPS analyses were carried out with a Kratos Axis Ultra^{DLD} spectrometer using a monochromatic Al Kα source, operated at 20 mA and 15 kV. Specimens for the XPS measurements were prepared by dropping a concentrated NC solution onto freshly cleaved highly oriented pyrolytic graphite substrates. Survey scan analyses were carried out with an analysis area of 300 × 700 μm and a pass energy of 160 eV. High resolution analyses were carried out over the same analysis area and a pass energy of 10 eV. The Kratos charge neutralizer system was used on all specimens. Spectra have been charge-corrected to the main line of the carbon 1s spectrum (adventitious carbon) set to 284.8 eV. Spectra were analyzed using CasaXPS software (version 2.3.17).

RESULTS AND DISCUSSION

Undoped $Cs_2AgInCl_6$ NCs. The synthesis of $Cs_2AgInCl_6$ NCs was performed using a colloidal hot-injection approach in which metal carboxylate precursors (i.e., Ag(ac), $In(ac)_3$, and Cs-oleate) are first dissolved in diphenyl ether together with ligands (Olam and OAc) and then reacted with benzoyl chloride (see Experimental Section for details). This technique allows for the fine adjustment of the ratio of the cation precursors, which react only upon injection of the chloride precursor. Working with a Cs/Ag/In/Cl molar ratio of 2/0.96/1/6.9, a pure double perovskite $Cs_2AgInCl_6$ phase (ICSD number 257115) was observed by XRD analysis of the NC product (Figure 1a). The elemental analysis, performed using a combination of ICP and XPS techniques, revealed an average stoichiometry of $Cs_{2.5}Ag_{0.9}In_{1.1}Cl_6$, which is compatible with the expected DP structure (Figure S1 and Table S1 of SI). The product consisted of 9.8 nm cubic-shaped NCs with a size distribution of ∼16% (±1.6 nm), as indicated from our TEM analysis (Figure 1b). The HRTEM micrographs of the synthesized NCs revealed that they are crystalline, with no

DOI: 10.1021/jacs.8b07983
J. Am. Chem. Soc. 2018, 140, 12989−12995

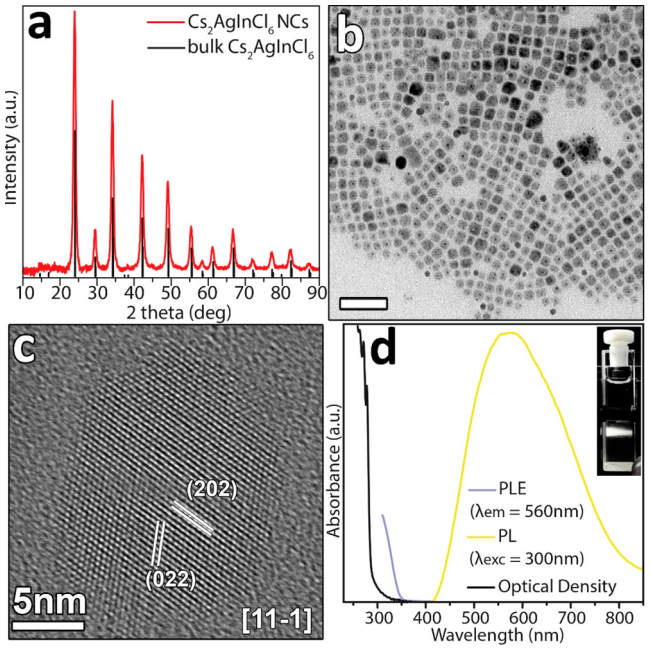

Figure 1. (a) XRD pattern of product NCs with the corresponding reflections of bulk $Cs_2AgInCl_6$ (ICSD number 257115). (b) Low-resolution TEM and (c) HRTEM micrographs of $Cs_2AgInCl_6$ NCs. The scale bar in panel (b) is 50 nm. The dark spots observed in individual nanocubes are metallic Ag formed by the electron beam during the observation. (d) Absorption, PL, and PL excitation (PLE) spectra of a $Cs_2AgInCl_6$ NCs dispersion in hexane, and a photo of the PL emission from the cuvette under Xe lamp excitation at 300 nm (inset).

obvious crystal defects, and that they exhibit lattice fringes compatible with the DP $Cs_2AgInCl_6$ structure (Figure 1c). Eventually our STEM-EDS analysis, performed on ensembles of NCs, further confirmed the expected $Cs_2AgInCl_6$ stoichiometry (Figures S2a and S3 and Table S2 of SI).

It is worth noting that both the XRD and the elemental analyses ruled out the presence of secondary products, which can easily form when dealing with the synthesis of multinary NC systems.[25,56] Indeed, when slightly different precursor ratios were employed, e.g., using a stoichiometric amount of Ag(ac), we noticed the formation of undesired AgCl (Figure S4b of SI). On the other hand, variation of the injection temperature, which was increased to 120 °C, resulted only in bigger NCs (14.8 nm) having a broader size distribution of 19% (±2.8) nm (Figure S4a of SI).

After the structural characterization of our DP NCs, we investigated their optical properties. As shown in Figure 1d, the absorption onset of $Cs_2AgInCl_6$ NCs was observed at around 350 nm with a strong increase in the absorbance only below ~290 nm. The Eg_{OPT}, calculated from the corresponding Tauc plot, fell at 4.38 eV, which is higher than 3.2−3.5 eV, values that are typically reported for this material (Figure S5 of SI).[7,23,36−38] The sample exhibited a weak and broad PL emission centered at 560 nm (PLQY ~ 1.6 ± 1%, see Table S3 of SI), which is also shifted to higher energies compared to those of previously reported bulk samples.[7,36,37] The PL was measured to originate from exciting the material at an energy close to its optical bandgap (290 nm, 4.27 eV), as evidenced by the corresponding PLE curve (Figure 1d). The blue shift of both absorption edge and PL emission of our $Cs_2AgInCl_6$ NCs compared to those of reported bulk samples suggested that our NCs are in the quantum confinement regime.

Next, we studied the stability of the as-synthesized DP NCs. Our NCs were stable in air, retaining their crystal structure even after several days of exposure (Figure S6 of SI), in line with what observed for bulk $Cs_2AgInCl_6$ materials. The thermal stability of our NCs was further investigated by DTA/TG coupled with evolved gas analysis (EGA). Two weight losses (for a total loss of 40%) were detected from 40 °C to 450 °C (Figure S7 of the SI). On the basis of the EGA, the evolved species, at this stage of the annealing, were identified as hexane, DPE, and ligands (Figure S8a of SI). The DTA curve identified a sharp endothermic peak at 462.5 °C, indicating the melting point of the DP NCs (Figure S7 of SI). The melting temperature observed here is lower than that of bulk $Cs_2AgInCl_6$ (~500 °C),[37] indicating a reduced or absent NCs coalescence. The reduced melting point of NCs compared to the bulk is additional manifestation of the size effect. At higher temperatures, further changes in the TG curve are associated with the decomposition of the DP material (Figure S7 of SI): a first loss was observed from ~500 °C to 810 °C and a second one from 810 °C to ~980 °C, in which 53% and 47% of the residual weight was lost, respectively. These were tentatively ascribed to the vaporization of $CsInCl_4$ and $CsAgCl_2$ that correspond to a theoretical loss of 56% and 44%, respectively. On the other hand, an univocal identification of the degradation products is not trivial due to the numerous possible binary compounds that might vaporize (i.e., CsCl, $InCl_3$, and AgCl).[7]

Overall our results revealed that, similar to their bulk counterparts, colloidal $Cs_2AgInCl_6$ NCs are thermally stable up to ~500 °C and are poor emitters, possibly due to the combination of a peculiar electronic structure,[7,30] defects, and surface states.

Mn-Doped $Cs_2AgInCl_6$ NCs. To exploit the good stability of $Cs_2AgInCl_6$ NCs and to attempt an enhancement of their emission, we decided to dope them with Mn^{2+} ions, inspired by the work of Nandha et al.[38] The doping was achieved by adding a desired amount of $Mn(ac)_2$ to the synthesis of $Cs_2AgInCl_6$ NCs while keeping all the other synthesis parameters fixed (see Experimental Section for details). The doped samples were prepared by employing two different In/Mn precursor ratios of 0.1 and 0.2, resulting in doping levels of 0.5% and 1.5%, respectively (as determined by elemental analyses via ICP and XPS, see Table S1 of SI; the reported percentages are of Mn ions with respect to the total number of atoms, i.e., Cs, In, Ag, Cl, and Mn). The doped samples will be referred as 0.5% and 1.5% Mn-doped in the remainder of the manuscript. Both samples consisted of cubic shaped NCs having a mean size of 11.6 ± 1.5 nm (0.5% Mn-doped sample) and 12.6 ± 2.6 nm (1.5% Mn-doped sample), as evidenced by our TEM analysis (Figure 2a,b). The HRTEM micrographs of Mn-doped $Cs_2AgInCl_6$ NCs revealed their DP structure, suggesting, also, that the inclusion of Mn ions did not induce the formation of crystal defects (Figure 2c,d). The XRD characterization of the Mn-doped samples confirmed that they crystallized in the DP $Cs_2AgInCl_6$ structure (ICSD number 257115), with the absence of undesired secondary phases (Figure 2e). STEM-EDS analyses performed on both samples detected the presence of Mn, with doping levels in line with what was measured by ICP and XPS, and, thus, confirming the effective doping of $Cs_2AgInCl_6$ NCs (Figures S2b,c, S9, and S10 and Table S2 of SI). In addition, considering that our NCs

DOI: 10.1021/jacs.8b07983
J. Am. Chem. Soc. 2018, 140, 12989−12995

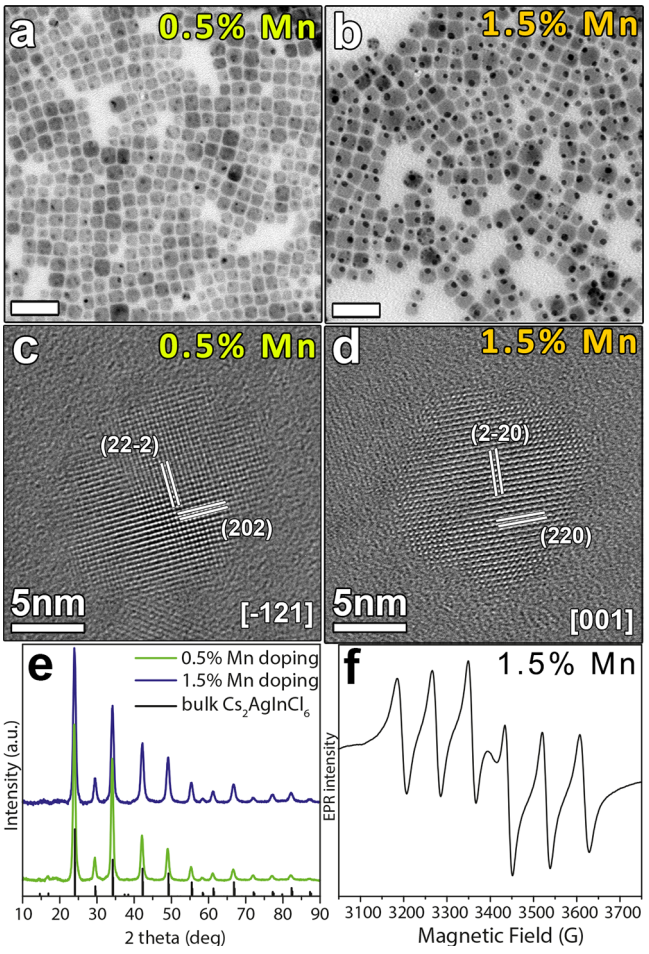

Figure 2. Low-resolution TEM (a, b) and HRTEM (c, d) micrographs of 0.5% and 1.5% Mn-doped $Cs_2AgInCl_6$ NCs. The scale bars in panels (a) and (b) are 50 nm. The dark spots observed in individual nanocubes are metallic Ag formed by electron beam irradiation during the observation. (e) XRD pattern of 0.5% and 1.5% Mn-doped $Cs_2AgInCl_6$ NCs with the corresponding reflections of bulk $Cs_2AgInCl_6$ (ICSD number 257115). (f) ESR spectrum of 1.5% Mn-doped $Cs_2AgInCl_6$ NCs, measured at room temperature.

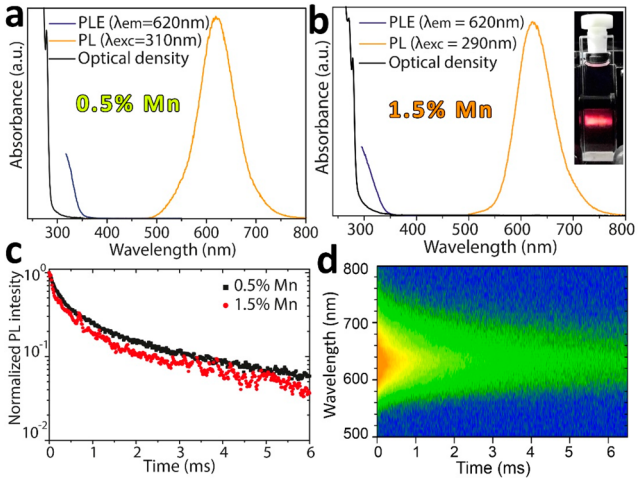

Figure 3. Absorption, PL, and PL excitation (PLE) spectra of (a) 0.5% and (b) 1.5% Mn-doped $Cs_2AgInCl_6$ NCs dispersions in hexane. The inset of panel b shows the corresponding optical image under Xe lamp excitation at 300 nm. (c) PL decay traces of Mn-doped $Cs_2AgInCl_6$ NCs collected at the emission maximum (620 nm) at room temperature. (d) Contour plot of the spectrally and time-resolved Mn^{2+} luminescence (logarithmic scale) of the 1.5% Mn-doped DP sample. In both c and d, the samples were excited at 355 nm.

are ~11−12 nm in size, and that EDS and XPS results are in agreement, we conclude that the Mn dopants are uniformly distributed inside the NCs, rather than being segregated at the surface.

A further confirmation of the presence of Mn dopants inside the $Cs_2AgInCl_6$ DP lattice comes from ESR analyses performed on the sample with the brightest PL (1.5% Mn-doped). ESR spectroscopy is a common technique used to understand the chemical environment of Mn^{2+} ions in host matrixes.[38,41,42] As shown in Figure 2f, the ESR spectrum of the Mn-doped sample evidenced the characteristic sextet due to isotropic hyperfine coupling of the electronic spin states with the nuclear spin of isolated Mn^{2+} ions, with a characteristic *g*-factor of 2.065 ± 0.001, and a hyperfine constant A of 8.4 ± 0.1 mT, thus confirming the incorporation of Mn^{2+} cations into the DP structure.

Similar to the undoped $Cs_2AgInCl_6$ NCs, the absorption onset of Mn-doped products was observed to be close to ~350 nm, with an Eg_{OPT}, calculated from the corresponding Tauc plots, of 4.36−4.38 eV (Figure 3a,b and Figure S5 of SI). On the other hand, both Mn-doped DP samples showed a broad PL band centered at ~620 nm due to the $^4T_1 \rightarrow {}^6A_1$ transition of Mn^{2+} dopants,[40,42−45] with a full-width-at-half-maximum ranging from 250 meV (1.5% Mn doped sample) to 270 meV (0.5% doped sample), slightly narrower than that reported by Nandha et al. (300 meV) (Figure 3a,b).[38] Time-resolved PL analysis, reported in Figure 3c,d, revealed a microsecond-long luminescence and, essentially, an invariance of the emission profile over time, consistent with the spin forbidden nature of the Mn^{2+} luminescence and indicating the lack of spectral diffusion due to intersite energy-transfer between Mn centers, despite the relatively high doping level.[40,42] Notably, PLE spectra revealed that in both samples such orange emission originated when exciting the NCs above 350 nm (Figure 3a,b), that is, at energies comparable to that of Eg_{OPT}, thus strongly suggesting that the Mn-PL is sensitized by energy transfer from the $Cs_2AgInCl_6$ host excitons, similar to that of previously reported Mn-doped semiconductors. The intensity of the PL emission of Mn-doped $Cs_2AgInCl_6$ NC samples increased with the doping level from 0.5% to 1.5% of Mn, with the highest PLQY measured among these samples of ~16 ± 4%, presently the highest reported value for double perovskite NC samples (see Table S3 of SI).

With the aim of increasing the doping level of our DP NCs, we also performed a control experiment using a Mn/In precursor ratio of 0.3. The resulting NC product exhibited the expected DP $Cs_2AgInCl_6$ crystal structure with no presence of undesired secondary products (Figure S11a,b of SI). On the other hand, our ICP, STEM-EDS, and XPS elemental analyses revealed that this sample had a Mn doping amount of ~1.5%, indicating that an increase of Mn precursor did not lead to any further inclusion of dopants (see Figure S2d, Tables S1 and S2 of SI). The optical features of these NCs, i.e., absorption, PL and PLE, and PL lifetime, were identical to those of the 0.5% and 1.5% Mn-doped samples, but with a PLQY of 7% (Figure S11c,d and Table S3 of SI). Overall, our control experiment suggested that (i) a maximum doping level of 1.5% could be achieved in such DP NC systems, and (ii) that a 0.2 Mn/In

DOI: 10.1021/jacs.8b07983
J. Am. Chem. Soc. 2018, 140, 12989−12995

precursor ratio optimized not only the doping level, but also the PLQY of the final NCs.

Next, we studied the thermal stability of our Mn-doped samples. The TG curves of such compounds were similar to that of the $Cs_2AgInCl_6$ NCs (Figure S8b of SI). Interestingly, the melting point of Mn-doped samples was found to increase linearly from 469.4 °C to 479.6 °C when increasing the doping level from 0.5% to 1.5% (Figure S7 of SI). It is noteworthy that the sample obtained using a Mn/In precursor ratio of 0.3 and the 1.5% Mn-doped one had the same melting temperature, suggesting that both products had the same doping levels, as indicated from our elemental analyses.

CONCLUSION

We have demonstrated an efficient colloidal route to synthesize $Cs_2AgInCl_6$ NCs with good control over the size distribution of the final product. The phase-pure NCs exhibited the expected double perovskite crystal structure, good stability under air, and a weak white PL emission (PLQY ~ 1.6 ± 1%). The synthesis was extended to the preparation of Mn-doped $Cs_2AgInCl_6$ NCs. The Mn-doped NC samples were characterized by the same double perovskite crystal structure, with no presence of undesired secondary phases. Our elemental analyses revealed that a Mn doping level as high as 1.5% could be achieved. The ESR analysis confirmed that Mn ions were effectively incorporated inside the DP structure. As a consequence of the doping, a bright PL emission characterized our DP NCs with a PLQY as high as ~16 ± 4%.

ASSOCIATED CONTENT

Supporting Information

The Supporting Information is available free of charge on the ACS Publications website at DOI: 10.1021/jacs.8b07983.

XPS spectra, summary of XPS, ICP, and EDS elemental analyses, STEM-EDS maps, TEM, XRD, HRTEM, and optical characterization data, Tauc plots, DTA and TG curves and evolved gas analysis data, and PLQY experimental details (PDF)

AUTHOR INFORMATION

Corresponding Authors

*luca.detrizio@iit.it

*liberato.manna@iit.it

ORCID

Federico Locardi: 0000-0002-1794-8282

Dmitry Baranov: 0000-0001-6439-8132

Mirko Prato: 0000-0002-2188-8059

Valerio Pinchetti: 0000-0003-3792-3661

Sergio Brovelli: 0000-0002-5993-855X

Luca De Trizio: 0000-0002-1514-6358

Liberato Manna: 0000-0003-4386-7985

Author Contributions

Federico Locardi and Matilde Cirignano contributed equally to this work.

Notes

The authors declare no competing financial interest.

ACKNOWLEDGMENTS

We acknowledge funding from the European Union under grant agreements no. 614897 (ERC grant TRANS-NANO). We thank Lea Pasquale for her support in the XPS analysis. We thank A. Olivati, M. Vitari and G. Maggi for their support in the spectroscopic experiments.

REFERENCES

(1) Akkerman, Q. A.; Rainò, G.; Kovalenko, M. V.; Manna, L. *Nat. Mater.* **2018**, *17*, 394−405.

(2) Saliba, M.; Matsui, T.; Seo, J.-Y.; Domanski, K.; Correa-Baena, J.-P.; Nazeeruddin, M. K.; Zakeeruddin, S. M.; Tress, W.; Abate, A.; Hagfeldt, A.; Gratzel, M. *Energy Environ. Sci.* **2016**, *9*, 1989−1997.

(3) Savory, C. N.; Walsh, A.; Scanlon, D. O. *ACS Energy Lett.* **2016**, *1*, 949−955.

(4) Swarnkar, A.; Ravi, V. K.; Nag, A. *ACS Energy Lett.* **2017**, *2*, 1089−1098.

(5) Jodlowski, A. D.; Rodríguez-Padrón, D.; Luque, R.; de Miguel, G. *Adv. Energy Mater.* **2018**, *8*, 1703120.

(6) Deng, Z.; Wei, F.; Sun, S.; Kieslich, G.; Cheetham, A. K.; Bristowe, P. D. *J. Mater. Chem. A* **2016**, *4*, 12025−12029.

(7) Zhou, J.; Xia, Z.; Molokeev, M. S.; Zhang, X.; Peng, D.; Liu, Q. *J. Mater. Chem. A* **2017**, *5*, 15031−15037.

(8) Volonakis, G.; Filip, M. R.; Haghighirad, A. A.; Sakai, N.; Wenger, B.; Snaith, H. J.; Giustino, F. *J. Phys. Chem. Lett.* **2016**, *7*, 1254−1259.

(9) Giustino, F.; Snaith, H. J. *ACS Energy Lett.* **2016**, *1*, 1233−1240.

(10) Ono, L. K.; Juarez-Perez, E. J.; Qi, Y. *ACS Appl. Mater. Interfaces* **2017**, *9*, 30197−30246.

(11) Wang, A.; Yan, X.; Zhang, M.; Sun, S.; Yang, M.; Shen, W.; Pan, X.; Wang, P.; Deng, Z. *Chem. Mater.* **2016**, *28*, 8132−8140.

(12) Dolzhnikov, D. S.; Wang, C.; Xu, Y.; Kanatzidis, M. G.; Weiss, E. A. *Chem. Mater.* **2017**, *29*, 7901−7907.

(13) Zhang, J.; Yang, Y.; Deng, H.; Farooq, U.; Yang, X.; Khan, J.; Tang, J.; Song, H. *ACS Nano* **2017**, *11*, 9294−9302.

(14) Park, B.-W.; Philippe, B.; Zhang, X.; Rensmo, H.; Boschloo, G.; Johansson, E. M. J. *Adv. Mater.* **2015**, *27*, 6806−6813.

(15) Jellicoe, T. C.; Richter, J. M.; Glass, H. F. J.; Tabachnyk, M.; Brady, R.; Dutton, S. E.; Rao, A.; Friend, R. H.; Credgington, D.; Greenham, N. C.; Böhm, M. L. *J. Am. Chem. Soc.* **2016**, *138*, 2941−2944.

(16) Zhao, X.-G.; Yang, J.-H.; Fu, Y.; Yang, D.; Xu, Q.; Yu, L.; Wei, S.-H.; Zhang, L. *J. Am. Chem. Soc.* **2017**, *139*, 2630−2638.

(17) Morss, L. R.; Siegal, M.; Stenger, L.; Edelstein, N. *Inorg. Chem.* **1970**, *9*, 1771−1775.

(18) Wei, F.; Deng, Z.; Sun, S.; Xie, F.; Kieslich, G.; Evans, D. M.; Carpenter, M. A.; Bristowe, P. D.; Cheetham, A. K. *Mater. Horiz.* **2016**, *3*, 328−332.

(19) Deng, Z.; Wei, F.; Brivio, F.; Wu, Y.; Sun, S.; Bristowe, P. D.; Cheetham, A. K. *J. Phys. Chem. Lett.* **2017**, *8*, 5015−5020.

(20) Slavney, A. H.; Hu, T.; Lindenberg, A. M.; Karunadasa, H. I. *J. Am. Chem. Soc.* **2016**, *138*, 2138−2141.

(21) McClure, E. T.; Ball, M. R.; Windl, W.; Woodward, P. M. *Chem. Mater.* **2016**, *28*, 1348−1354.

(22) Filip, M. R.; Hillman, S.; Haghighirad, A. A.; Snaith, H. J.; Giustino, F. *J. Phys. Chem. Lett.* **2016**, *7*, 2579−2585.

(23) Tran, T. T.; Panella, J. R.; Chamorro, J. R.; Morey, J. R.; McQueen, T. M. *Mater. Horiz.* **2017**, *4*, 688−693.

(24) Bekenstein, Y.; Dahl, J. C.; Huang, J.; Osowiecki, W. T.; Swabeck, J. K.; Chan, E. M.; Yang, P.; Alivisatos, A. P. *Nano Lett.* **2018**, *18*, 3502−3508.

(25) Creutz, S. E.; Crites, E. N.; De Siena, M. C.; Gamelin, D. R. *Nano Lett.* **2018**, *18*, 1118−1123.

(26) Yang, B.; et al. *Angew. Chem., Int. Ed.* **2018**, *57*, 5359−5363.

(27) Wu, C.; et al. *Advanced Science* **2018**, *5*, 1700759.

(28) Gao, W.; et al. *ChemPhysChem* **2018**, *19*, 1696−1700.

(29) Feng, H.-J.; Deng, W.; Yang, K.; Huang, J.; Zeng, X. C. *J. Phys. Chem. C* **2017**, *121*, 4471−4480.

(30) Meng, W.; Wang, X.; Xiao, Z.; Wang, J.; Mitzi, D. B.; Yan, Y. *J. Phys. Chem. Lett.* **2017**, *8*, 2999−3007.

(31) Du, K.-z.; et al. *Angew. Chem., Int. Ed.* **2017**, *56*, 8158−8162.

DOI: 10.1021/jacs.8b07983
J. Am. Chem. Soc. 2018, 140, 12989−12995

(32) Lei, L.-Z.; Shi, Z.-F.; Li, Y.; Ma, Z.-Z.; Zhang, F.; Xu, T.-T.; Tian, Y.-T.; Wu, D.; Li, X.-J.; Du, G.-T. *J. Mater. Chem. C* **2018**, *6*, 7982−7988.
(33) Pantaler, M.; Cho, K. T.; Queloz, V. I. E.; García Benito, I.; Fettkenhauer, C.; Anusca, I.; Nazeeruddin, M. K.; Lupascu, D. C.; Grancini, G. *ACS Energy Lett.* **2018**, *3*, 1781−1786.
(34) Jain, A.; Voznyy, O.; Sargent, E. H. *J. Phys. Chem. C* **2017**, *121*, 7183−7187.
(35) Zhao, X.-G.; Yang, D.; Sun, Y.; Li, T.; Zhang, L.; Yu, L.; Zunger, A. *J. Am. Chem. Soc.* **2017**, *139*, 6718−6725.
(36) Volonakis, G.; Haghighirad, A. A.; Milot, R. L.; Sio, W. H.; Filip, M. R.; Wenger, B.; Johnston, M. B.; Herz, L. M.; Snaith, H. J.; Giustino, F. *J. Phys. Chem. Lett.* **2017**, *8*, 772−778.
(37) Luo, J.; Li, S.; Wu, H.; Zhou, Y.; Li, Y.; Liu, J.; Li, J.; Li, K.; Yi, F.; Niu, G.; Tang, J. *ACS Photonics* **2018**, *5*, 398−405.
(38) Nandha, K. N.; Nag, A. *Chem. Commun.* **2018**, *54*, 5205−5208.
(39) Xu, J.; Liu, J.-B.; Liu, B.-X.; Huang, B. *J. Phys. Chem. Lett.* **2017**, *8*, 4391−4396.
(40) De, A.; Mondal, N.; Samanta, A. *Nanoscale* **2017**, *9*, 16722−16727.
(41) Buonsanti, R.; Milliron, D. J. *Chem. Mater.* **2013**, *25*, 1305−1317.
(42) Guria, A. K.; Dutta, S. K.; Adhikari, S. D.; Pradhan, N. *ACS Energy Lett.* **2017**, *2*, 1014−1021.
(43) Yang, H.; Santra, S.; Holloway, P. H. *J. Nanosci. Nanotechnol.* **2005**, *5*, 1364−1375.
(44) Xu, K.; Meijerink, A. *Chem. Mater.* **2018**, *30*, 5346−5352.
(45) Pradhan, N. *ChemPhysChem* **2016**, *17*, 1087−1094.
(46) Bhargava, R. N.; Gallagher, D.; Hong, X.; Nurmikko, A. *Phys. Rev. Lett.* **1994**, *72*, 416−419.
(47) Pradhan, N.; Peng, X. *J. Am. Chem. Soc.* **2007**, *129*, 3339−3347.
(48) Nag, A.; Chakraborty, S.; Sarma, D. D. *J. Am. Chem. Soc.* **2008**, *130*, 10605−10611.
(49) Meinardi, F.; Akkerman, Q. A.; Bruni, F.; Park, S.; Mauri, M.; Dang, Z.; Manna, L.; Brovelli, S. *ACS Energy Lett.* **2017**, *2*, 2368−2377.
(50) Akkerman, Q. A.; Gandini, M.; Di Stasio, F.; Rastogi, P.; Palazon, F.; Bertoni, G.; Ball, J. M.; Prato, M.; Petrozza, A.; Manna, L. *Nat. Energy* **2017**, *2*, 16194.
(51) Palazon, F.; Dogan, S.; Marras, S.; Locardi, F.; Nelli, I.; Rastogi, P.; Ferretti, M.; Prato, M.; Krahne, R.; Manna, L. *J. Phys. Chem. C* **2017**, *121*, 11956−11961.
(52) Yang, J. *Adv. Mater.* **2016**, *28*, 1176−1207.
(53) Gonzalez-Carrero, S.; Schmidt, L. C.; Rosa-Pardo, I.; Martínez-Sarti, L.; Sessolo, M.; Galian, R. E.; Pérez-Prieto, J. *ACS Omega* **2018**, *3*, 1298−1303.
(54) Imran, M.; Caligiuri, V.; Wang, M.; Goldoni, L.; Prato, M.; Krahne, R.; De Trizio, L.; Manna, L. *J. Am. Chem. Soc.* **2018**, *140*, 2656−2664.
(55) Kotz, J. C.; Treichel, P. M.; Townsend, J.; Treichel, D. *Chemistry & Chemical Reactivity*. 9th ed.; Cengage Learning Inc.: Boston, MA, 2014.
(56) De Trizio, L.; Manna, L. *Chem. Rev.* **2016**, *116*, 10852−10887.

DOI: 10.1021/jacs.8b07983
J. Am. Chem. Soc. 2018, 140, 12989−12995